

DAS3R: Dynamics-Aware Gaussian Splatting for Static Scene Reconstruction

Kai Xu¹, Tze Ho Elden Tse¹, Jizong Peng², Angela Yao¹

¹National University of Singapore ²dConstruct Robotics

{kxu, eldentse, ayao}@comp.nus.edu.sg jizong.peng@dconstruct.ai

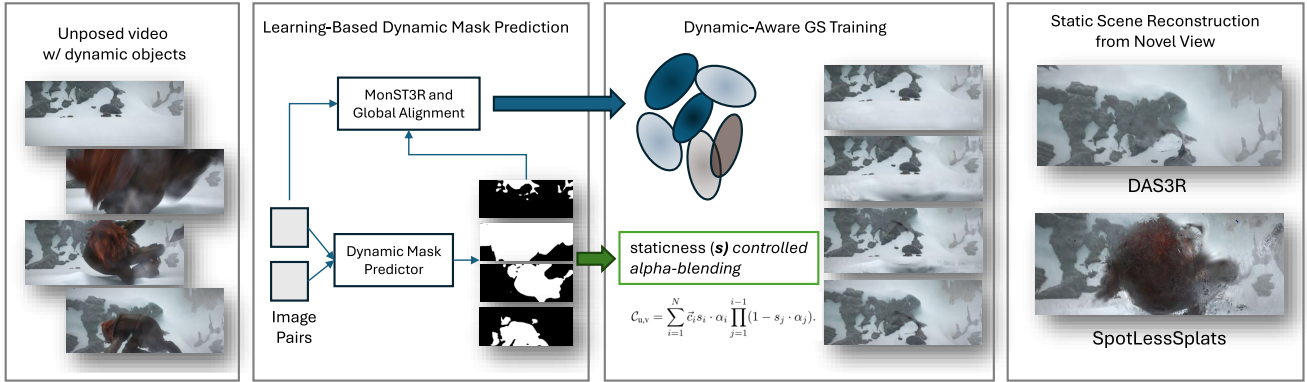


Figure 1. **Overview:** DAS3R featuring reconstructing static scene from unposed videos where dynamic objects occupy a significant portion of the scene. We predict dynamic mask directly from deep network with image pair as input. The predicted dynamic masks are then used for dynamic-aware Gaussian splatting training. In the figure we show an example from Sintel dataset. Compared to SpotLessSplats [18], DAS3R can reconstruct clean background while SpotLessSplats fails to remove the dynamic object.

Abstract

We propose a novel framework for scene decomposition and static background reconstruction from everyday videos. By integrating the trained motion masks and modeling the static scene as Gaussian splats with dynamics-aware optimization, our method achieves more accurate background reconstruction results than previous works. Our proposed method is termed DAS3R, an abbreviation for *Dynamics-Aware Gaussian Splatting for Static Scene Reconstruction*. Compared to existing methods, DAS3R is more robust in complex motion scenarios, capable of handling videos where dynamic objects occupy a significant portion of the scene, and does not require camera pose inputs or point cloud data from SLAM-based methods. We compared DAS3R against recent distractor-free approaches on the DAVIS and Sintel datasets; DAS3R demonstrates enhanced performance and robustness with a margin of more than 2 dB in PSNR. The project’s webpage can be accessed via <https://kai422.github.io/DAS3R/>

1. Introduction

Reconstructing static scenes from dynamic environments is a fundamental task in computer vision, with wide-ranging

applications in robotic perception, animation, and the metaverse. Current methods mainly focus on autonomous driving videos [10, 14], or unconstrained images with transient dynamic objects [8, 18, 24], where dynamic elements typically occupy a small portion of the scene. These methods struggle when applied to a broader range of everyday video content that involves continuous and substantial dynamic components as well as complex camera movements. Reconstructing static background from unposed everyday video presents multiple challenges. Primarily, the movement of large dynamic objects can influence the precision of camera pose estimation. Some methods [2, 17, 24, 30, 31] use segmentation networks to identify and exclude objects in video frames, but these methods often produce high false-positive rates, as semantically meaningful segmented objects are not necessarily dynamic. Other methods, such as NeRF-based or Gaussian Splatting-based dynamic scenes reconstruction [9, 12], rely on thresholding epipolar errors to distinguish static and dynamic regions, with camera poses computed by robust SLAM [28] and RANSAC [5] for statistical outlier rejection. This method proves inadequate when a significant portion of the scene consists of dynamic objects, resulting in the statistical majority shifting from the static background to dynamic content. By integrating depth data, [32] calculates an error map by contrasting the derived opti-

cal flow with the induced flow deduced from estimated camera poses, generating a dynamic mask by applying a threshold to this error. However, their performance significantly relies on accurate optical flow estimation and shows high sensitivity to the selection of threshold parameters.

We propose a direct learning-based approach to handle dynamic objects in scenes. By taking two frames of the same scene captured at different times as input and adopting MonST3R [32] as the backbone network, the dynamic mask can be accurately predicted even if it occupies a significant portion of the scene. The pairwise masks are subsequently aggregated into video-level dynamic masks by combining predictions from all chosen image pairs. The primary insight is to predict a dynamic mask from an image pair instead of relying on a single image. By employing comparison and cross-attention between the two images, the underlying camera poses are decomposed from object motion in the latent space, resulting in enhanced robustness in dynamic prediction. Our method uses ground-truth dynamic object masks to supervise the learning process with the synthetic dataset Point Odyssey [33], and is capable of generalizing to unseen datasets such as Sintel [3] and DAVIS [15]. We follow the same post-processing pipeline of MonST3R and DUST3R [26] to generate dense prediction and camera pose estimation of the video. By replacing the static confidence of MonST3R in the global alignment pipeline with model predicted dynamic masks, we achieve enhanced accuracy in scene depth reconstruction and camera pose estimation. Dense predictions are subsequently employed to initialize Gaussian splats, while the predicted dynamic masks drive the dynamic-aware training for Gaussian splatting.

To achieve static background reconstruction, current efforts in robust and distractor-free reconstruction often rely on semantic features and segmentation [8, 11, 18] and perform an implicit way to identify the transient components. While our method incorporated model predicted dynamic mask as the prior for decomposing the scene. This helps our framework to handle the persistent dynamics; we further incorporate Gaussian Splatting training with optimizable dynamic-aware attribute - the staticness. During the rendering stage, staticness directly contributes to the computation of Gaussian point colors through alpha blending. This allows efficient removal of dynamic elements and acts as a robust solution for mitigating false-positive predictions in dynamic mask assessments.

We compared our method against recent distractor-free reconstruction methods on the DAVIS and Sintel datasets; our approach achieves a performance improvement of over 2 dB on PSNR, exhibiting strong reconstruction capabilities even with complex camera movements and substantial dynamic elements. We summarize our contributions as follows:

- DAS3R can predict more accurate dynamic masks from image pairs compared to the static confidence offered by previous methods.
- Integrating staticness as a Gaussian point attribute, DAS3R achieves effective dynamic object suppression, and accurate reconstruction under complex camera movements and substantial dynamic elements.
- Detailed experimental results on DAVIS and Sintel datasets shows enhanced performance compared to distractor-free Gaussian Splatting approaches.

2. Related works

Dynamic Scene Decomposition. Estimating poses and reconstructing in dynamic settings often hinge on the segmentation of dynamic objects. Certain methods [9, 12] apply epipolar constraints to identify dynamic regions, relying on RANSAC for essential matrix estimation, which typically demands highly accurate correspondences. When the optical flow presented is imprecise, these methods find it challenging to decide whether the residual error arises from object movement or from faulty correspondences. Different approaches [2, 17, 24, 30, 31] emphasize the tracking and semantic segmentation of dynamic objects, generally relying on assumptions like the motion of foreground objects versus a static background, or the prior identification of mobile objects. However, these assumptions limit their applicability.[1] An alternative approach presumes that both motion segmentation and reconstruction can be concurrently addressed using factorization methods like singular value decomposition (SVD), which separate camera and object motions. Regrettably, these approaches are frequently susceptible to noise and outliers. Our method decomposes dynamic scenes by segmentation but offers enhanced robustness and generalization by harnessing substantial volumes of training data. This allows us to reduce sensitivity to noise and outliers, thereby delivering a more scalable approach to comprehending dynamic scenes.

End-to-end Reasoning for 3D geometry. End-to-end reasoning aims to build a differentiable Structure-from-Motion (SfM) pipeline to replicate traditional workflows while enabling end-to-end training [21, 23, 25]. They leverage image pairs, which is the minimal input set required for multi-view geometric computation. Models such as DUST3R and MonST3R [26, 32] are capable of directly learning 3D pointmaps without intrinsic parameters as input. MonST3R extends DUST3R to dynamic scenes, directly regressing 3D point clouds across time steps from image pairs. DAS3R relies on MonST3R to predict dynamic masks for image pairs, and construct dynamic masks for the entire video through global alignment over frame pair graph and aggregation.

Distractor-free 3D Gaussian Splatting. The traditional 3DGS approach typically assumes inter-view consistency while this assumption can be violated when dealing with

dynamic objects. Recent methods have addressed the challenge by incorporating robust 3DGS training strategies to ignore transient interferences [8, 11, 14, 18, 22, 24]. For instance, WildGaussians [8] combines robust DINO features with an appearance modeling module to effectively handle occlusions and appearance variations in 3DGS. SpotLessSplats [18] leverages Stable Diffusion features and robust optimization techniques to suppress transient interferences in 3DGS. Similarly, HybridGS [11] introduces a hybrid model that integrates a multi-view-consistent 3D Gaussian model with a single-view-independent 2D Gaussian model, enabling the separation of transient and static elements in a scene.

In contrast, DAS3R focuses on capturing persistent and substantial dynamic objects from video data, while earlier approaches primarily focusing on transient dynamic objects from image data. Furthermore, DAS3R does not need camera parameters as input, while previous methods often rely on camera predictions provided by COLMAP as input.

3. Preliminary

3.1. 3D Gaussian Splatting

3D Gaussian Splatting [6] is a framework that represents a scene as a collection of 3D Gaussians. Each Gaussian $G(\vec{x})$ is parameterized by its mean position $\vec{\mu}$, covariance matrix Σ , color \vec{c}_i , and opacity α :

$$G(\vec{x}) = \exp\left(-\frac{1}{2}(\vec{x} - \vec{\mu})^\top \Sigma^{-1}(\vec{x} - \vec{\mu})\right). \quad (1)$$

The rendering process of 3DGS involves projecting 3D Gaussian primitives onto the 2D image plane. The contribution of each Gaussian to the rendered image is determined by integrating its density along the viewing direction, weighted by its opacity α and color attributes \vec{c}_i :

$$\mathcal{C}_{u,v} = \sum_{i=1}^N \vec{c}_i \alpha_i \prod_{j=1}^{i-1} (1 - \alpha_j). \quad (2)$$

where $\mathcal{C}_{u,v}$ denotes the final rendered color at pixel coordinate (u, v) , N is the number of all overlapping Gaussians.

The differentiable rasterization blends the contributions of all Gaussians in the scene based on their projection onto the image plane, resulting in a continuous and differentiable image representation. Through photometric loss, each Gaussian attribute can be optimized through gradient descent based on the rendered and ground truth images.

$$\mathcal{L}_{\text{loss}} = \mathcal{L}_{\text{pixel}} + \lambda_{\text{ssim}} \cdot \mathcal{L}_{\text{ssim}}, \quad (3)$$

Here, $\mathcal{L}_{\text{pixel}} = \|\mathcal{I} - \hat{\mathcal{I}}\|_1$ signifies the photometric loss calculated pixel-by-pixel, and $\mathcal{L}_{\text{ssim}} = \mathcal{S}_{\text{ssim}}(\mathcal{I}, \hat{\mathcal{I}})$ corresponds to the loss based on structural similarity. Recently,

MonoGS [13] has also allowed for the simultaneous refinement of camera poses and Gaussian splats.

The presence of dynamic content in a scene results in inconsistencies for Gaussian training objectives when captures are taken at different timestamps. DAS3R employs optimizable dynamic masks to explicitly decompose the loss, directing the influence from the static scene flow solely back to the Gaussian parameters.

4. Methodology

4.1. Problem Definition

Given a with a casual captured dynamic video, our objective is to reconstruct a 3D Gaussian model of the static background, which allows for rendering that background from any viewpoint. To achieve this, we intend to train a 3D Gaussian model utilizing a dataset comprising RGB videos $\mathcal{I} = \{I_i \mid i = 1, \dots, N\}$. Notably, the dataset for training does not include individual frame camera poses, depth details, and camera intrinsic parameters.

Each frame I_i encompasses not only photometric changes due to homography transformation caused by ego-centric camera movement but also includes changes from the motion of dynamic objects. A similar setting is the distractor-free Gaussian Splatting [8, 18], aimed at removing transient objects for the reconstruction process from unrestrained images. In contrast to their scenarios where the dynamic objects are only transient and limited in scale, our approach tackles the challenge of reconstructing static scenes from complex dynamic videos, which involve persistent and significant dynamic objects along with intricate camera movements, as seen in the DAVIS [15] and Sintel [3].

4.2. Camera Pose Estimation under Dynamic Scene

Estimating depth and camera poses from dynamic videos poses a chicken-and-egg problem. The interplay between the motion of dynamic entities and the motion of the scene is inherently entangled. For instance, when using Gaussian Splatting to reconstruct a casual video, a 2D reprojection loss can be employed to simultaneously optimize both camera poses and the appearance of dynamic objects. When back-propagating photometric error to scene appearance and camera parameters concurrently, an ambiguity emerges regarding whether the observed changes are due to camera movement or object motion.

Previous research efforts have focused on separating camera motion from object motion through the use of epipolar error [9, 12] and segmentation methods based on optical flow [27]. The technique presented in MonST3R [32] also calculates induced flow from the estimated camera motion and depth, and subsequently determines errors based on estimated optical flow. These approaches rely heavily on

precise optical flow predictions and the tuning of hyperparameters for error thresholding. Moreover, some methods [24] utilize semantic segmentation techniques like Segment Anything [7], which depend on predictions from single images under the assumption that dynamic objects form the semantic foreground, an assumption that often does not hold in real-world contexts.

Dynamic region segmentation We propose a method to train dynamic segmentation masks directly from image pair inputs. Unlike traditional semantic segmentation networks that rely on a single image for predictions, our dynamic approach relies on reasoning across two overlapping image frames. In particular, we employ MonST3R as the foundational model for predicting the dynamic masks. Adopting the approach of DUSt3R[26] and CroCo v2 [29], MonST3R performs direct regression of dense 3D point maps from the image pairs exhibiting dynamic content, eliminating the need for prior scene or camera information, such as intrinsic parameters.

Specifically, the input consists of two RGB images with some overlapping content, I_n and I_m , captured at different time points t_n and t_m , where $I_n, I_m \in \mathbb{R}^{W \times H \times 3}$. The output includes two corresponding point maps $\mathbf{X}^{(n,n)}$ and $\mathbf{X}^{(n,m)} \in \mathbb{R}^{W \times H \times 3}$, and associated confidence maps $\mathbf{C}^{(n,n)}, \mathbf{C}^{(m,n)}$. The first subscript indicates the coordinate system of the point maps, which are both expressed in the same coordinate system as the image I_1 , while the second subscript indicates the frame index of the point map. In addition to MonST3R, we also predict a dynamic mask $\mathbf{M}^{(n,n)} \in \mathbb{R}^{W \times H \times 1}$ that designates whether points are part of a dynamic object region. For saving computations, we only predict the dynamic mask for frame 1 as it is sufficient to be aggregated to image dynamic masks. The dynamic mask prediction, which employs the DPT head [16], utilizes intermediate features derived from CroCo backbones. This includes the encoded features from each image and the cross-attention output’s intermediate features. For successful training of this model, we produce ground-truth dynamic masks for Point Odyssey [33]. Point Odyssey provides sparse 3D points motion information based on its 3D trajectories, from which we can generate the image-level dynamic mask by nearest interpolation to the image pixel’s 3D projection.

Comparison to MonST3R We perform both qualitative and quantitative comparisons with static confidence from MonST3R as shown in Table 1 and Figures 2 and 3. Our approach delivers more accurate segmentation results, whereas MonST3R often either misses segments or incorrectly identifies static areas as dynamic. One limitation of our model’s prediction mask is the occurrence of false positives in scenarios involving significant depth variation, which complicates the differentiation between static and dynamic foregrounds. To address this challenge, we integrate

Method	DAVIS	Sintel
MonST3R	32.5	37.1
Ours	39.7	59.3

Table 1. Comparison of dynamic mask accuracy (IoU) on DAVIS and Sintel datasets.

staticness into the Gaussian property and further refine it during training. More details are provided in Section 4.3.

Figure 2. Dynamic Mask Comparison on DAVIS dataset.

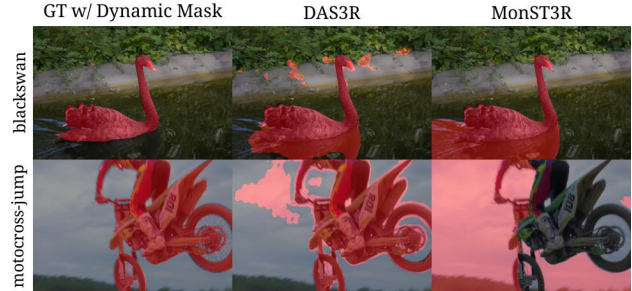
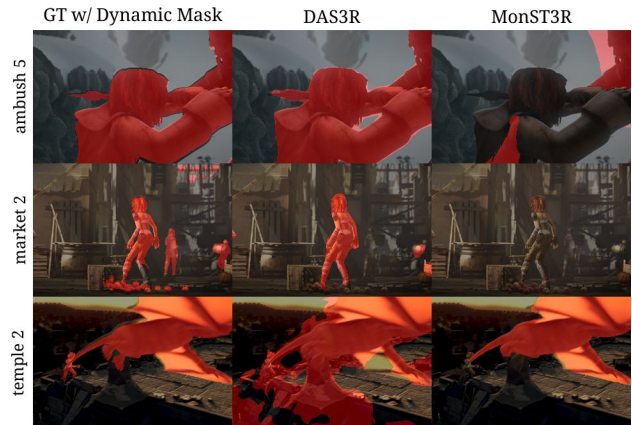


Figure 3. Dynamic Mask Comparison on Sintel dataset.



4.2.1 Global Alignment with Predicted Dynamic Mask

We follow DUSt3R [26] and MonST3R [32] in transforming pair predictions into the video’s global camera poses. DUSt3R introduced a global alignment loss, while MonST3R proposed an approach involving optical flow reprojection loss and smoothing loss, utilizing optimized static confidence to adjust the loss. In our approach, we replace static confidence by directly aggregating pairwise dynamic mask predictions into image dynamic masks.

Let $\mathcal{G}(\mathcal{V}, \mathcal{E})$ be the connectivity graph of the frames’ indices. \mathcal{V} denotes vertices and \mathcal{E} denotes edges, where each edge $e = (n, m) \in \mathcal{E}$ denotes pair images I^n and I^m which share similar visual content for pointmap computation.

For each image pair $e = (n, m) \in \mathcal{E}$, the pairwise pointmaps $\mathbf{X}^{(n,n)}, \mathbf{X}^{(m,n)}$, associated confidence maps $\mathbf{C}^{(n,n)}, \mathbf{C}^{(m,n)}$, and soft dynamic mask $\mathbf{M}^{(n,n)}$.

Let us assume the optimal global pointmap at time t is $\mathbf{X}^{(t,w)}$, the first t denotes frame index and the second W denotes that the pointmap is under the world coordinates, for edge (m, n) ,

$$\mathcal{L}_{\text{align}}(\mathbf{X}^{(\cdot,w)}, \sigma, \mathcal{G}(\mathcal{V}, \mathcal{E})) = \sum_{e=(n,m) \in \mathcal{E}} \left(\|\mathbf{C}^{(n,n)}(\mathbf{X}^{(n,w)} - \sigma^e \mathbf{P}^n \mathbf{X}_e^{(n,n)})\|_1 + \|\mathbf{C}^{(m,n)} \cdot (\mathbf{X}^{(m,w)} - \sigma^e \mathbf{P}^n \mathbf{X}_e^{(m,n)})\|_1 \right), \quad (4)$$

σ^e denotes a pairwise scale factor, and \mathbf{P}^n is the camera pose transformation at frame n . Apart from pointmap alignment loss, we also use the smoothness loss from MonST3R for encouraging smooth camera motion: $\mathcal{L}_{\text{smooth}}(\mathbf{X}) = \sum_{t=0}^N (\|\mathbf{R}^{t\top} \mathbf{R}^{t+1} - \mathcal{I}\|_f + \|\mathbf{R}^{t\top} (\mathbf{T}^{t+1} - \mathbf{T}^t)\|_2)$, where $\|\cdot\|_f$ denotes the Frobenius norm, and \mathcal{I} is the identity matrix.

Flow loss with predicted dynamic mask In MonST3R, the flow projection loss aims for the global pointmaps and camera positions to align with the calculated flow concerning the confident static areas of the real frames, depending on determining static confidence regions using PnP and RANSAC. We replace the static confidence regions with our model’s dynamically predicted masks.

$$\mathcal{L}_{\text{flow}}(\mathbf{X}) = \sum_{W^i \in W} \sum_{t \rightarrow t' \in W^i} \|(1 - \mathbf{M}^t) \cdot (\mathbf{F}_{\text{cam}}^{t \rightarrow t'} - \mathbf{F}_{\text{est}}^{t \rightarrow t'})\|_1, \quad (5)$$

where $\mathbf{F}_{\text{cam}}^{t \rightarrow t'}$ is the induced flow and $\mathbf{F}_{\text{est}}^{t \rightarrow t'}$ is the estimated flow. \mathbf{M}^t is the aggregated masks from all pairs including frame t . *i.e.*

$$\mathbf{M}^t = \sum_{(t,m) \in \mathcal{E}_{t*}} \mathbf{M}^{t,t} / |\mathcal{E}_{t*}|, \quad (6)$$

where $|\cdot|$ denotes the cardinality of the set. The complete optimization for our dynamic global point cloud and camera poses is $\hat{\mathbf{X}} = \arg \min_{\mathbf{X}, \mathbf{P}_W, \sigma} \mathcal{L}_{\text{align}} + w_{\text{smooth}} \mathcal{L}_{\text{smooth}} + w_{\text{flow}} \mathcal{L}_{\text{flow}}$, where $w_{\text{smooth}}, w_{\text{flow}}$ are hyperparameters.

Evaluation on Sintel and TUM-dynamics Table 2 presents a comparison of camera pose estimation results on the Sintel and TUM-dynamics datasets. Integrating trained dynamic masks into the optimization process significantly enhances the overall accuracy of the camera pose, with notable improvements in rotation accuracy.

4.3. Static Background Reconstruction with 3D Gaussian Splating

We begin initializing the Gaussian splats by utilizing prediction from global alignment, integrating both the depths

Table 2. Evaluation of camera pose estimation on Sintel and TUM-dynamic datasets.

Method	Sintel			TUM-dynamics		
	ATE ↓	RPE trans ↓	RPE rot ↓	ATE ↓	RPE trans ↓	RPE rot ↓
Robust-CVD	0.360	0.154	3.443	0.153	0.026	3.528
CasualSAM	0.141	0.035	0.615	0.071	0.010	1.712
MonST3R*	0.108	0.042	0.732	0.104	0.022	1.042
Ours	0.107	0.041	0.669	0.072	0.019	0.948

* The results for MonST3R on TUM-dynamics are reproduced by us.

and camera parameters for each frame. Following InstantSplat [4], the dense 3D point clouds are filtered based on the model’s confidence values. Furthermore, each 3D Gaussian is linked with its accumulated dynamic probability \mathbf{M} , and this is added as an attribute of the Gaussian splats.

Specifically, **staticness** (s) is defined as the complement of the dynamic mask probability (P_{dynamic}):

$$s_{u,v,t} = 1 - \mathbf{M}_{u,v}^t, \in [0, 1]$$

where u, v denotes the pixel index of the initialization.

To address errors and noise in the predicted, especially false-positive segmentations in scenes with significant depth variation, we optimize the staticness property as an attribute of the Gaussian primitives. Each Gaussian is assigned an attribute called **staticness** (s), which quantifies the likelihood that the Gaussian primitive belongs to the static region. During rendering, the staticness is incorporated into the alpha blending computation to filter out dynamic objects when reconstructing static scenes.

The final alpha value for rendering is computed by:

$$\mathcal{C}_{u,v} = \sum_{i=1}^N \tilde{c}_i s_i \cdot \alpha_i \prod_{j=1}^{i-1} (1 - s_j \cdot \alpha_j). \quad (7)$$

Incorporating staticness into the Gaussian representation, DAS3R successfully diminishes the impact of dynamic objects and corrects false-positive predictions of dynamic masks, improving the reconstruction quality of static scenes.

Static alignment for camera poses refinement. In Section 4.2, we presented the loss functions used by MonST3R for achieving global alignment. These losses arise from analyzing local 3D point clouds constructed from depth information in each frame, with optimization performed on an individual frame level rather than across the full global point cloud space of the video. Nonetheless, aligning within the global 3D space poses two significant challenges: 1) the 3D point clouds for individual frames are discrete and created by reprojecting pixels, thus complicating accurate alignment, and 2) the inherently dynamic nature of the content opposes alignment.

To achieve global alignment of 3D geometries, we employ 3D Gaussians as the global representation for the entire

scene. By aligning the static components of the scene, the accuracy of camera pose estimation can be enhanced, leading to improved reconstruction quality. The alignment loss is defined as the L_1 loss on the rendered image, calculating the pixel-wise discrepancy between the rendered image $\mathbf{I}_{\text{rendered}}$ and the actual image \mathbf{I}_{gt} .

$$\mathcal{L}_{\text{image}} = \frac{1}{|\Omega|} \sum_{\mathbf{p} \in \Omega} \|\mathbf{I}_{\text{rendered}}(\mathbf{p}) - \mathbf{S}(\mathbf{p}) \cdot \mathbf{I}_{\text{gt}}(\mathbf{p})\|_1, \quad (8)$$

where $\mathbf{S}(\mathbf{p})$ denotes per-frame Staticness. Ω is the set of all pixels in the image, and \mathbf{p} is the 2D pixel coordinate.

Throughout the optimization, gradients are back-propagated to the camera pose parameters (\mathbf{R}_i for rotation and \mathbf{t}_i for translation) by re-projecting observed points into the Gaussian model.

Training. During the Gaussian optimization process, we allow only the position and opacity of the Gaussians to be optimized, while keeping their color parameters, rotation, and scale fixed. The opacities are initially set to $1/N$, with N representing the total number of frames, to ensure that gradients are propagated across all points in the scene. Since a sufficient number of initialization points have already been obtained during the initialization phase, we disable further cloning of Gaussians. Table 5 demonstrates that this strategy effectively accelerates the convergence of camera pose predictions while already achieving photometric performance that surpasses the baseline.

5. Experiment

5.1. Experimental Details

Training of dynamic mask network. We utilize the pre-trained model of DUST3R, keeping the ViT encoder and decoder fixed, while training the DPT head for dynamic mask prediction network. Following the approach of MonST3R, we train for a total of 50 epochs, using 20,000 sampled image pairs per epoch. We employ the AdamW optimizer with a learning rate of 5×10^{-5} and a mini-batch size of 4 per GPU. For the dataset, we use Point Odyssey [33], which is a dataset of 200k synthetic images that feature 131 realistic indoor and outdoor scenes.

We utilize the trajectories of ground truth points (which are sparse) to calculate the ground-truth dynamic mask. Since the points generated by the network are inverse-projected from the 2D pixel image onto 3D space, they do not completely align with the ground truth points. We apply nearest interpolation using points that possess dynamic indicators.

5.2. Static Scene Reconstruction

We use the Sintel [3] and DAVIS [15] datasets as the benchmark for our experiments. The Sintel dataset is a synthetic

dataset which is well-known for its dynamic complexity, featuring challenging scenes with intricate motion patterns and interactions between dynamic and static elements, making it ideal for evaluating dynamic video decomposition and reconstruction methods. The DAVIS dataset is a benchmark dataset widely used for video object segmentation tasks. From DAVIS 2016, we selected the initial 50 frames from 8 sequences wherein the ground-truth masks exclusively delineate the moving objects.

In our experiments, we report PSNR for novel static scene reconstruction. Since the Sintel and DAVIS datasets do not provide ground-truth backgrounds, we exclude dynamic objects from the PSNR calculation by applying the ground-truth dynamic mask. In the case of Sintel, these dynamic masks are generated using ground-truth camera poses and optical flow information. We implement a 90-10 split: 90% of the frames are designated for Gaussian model training, and the remaining 10% are designated as test frames for assessing PSNR. Additionally, during training, we refine the camera poses of test frames to ensure precise rendering during evaluation.

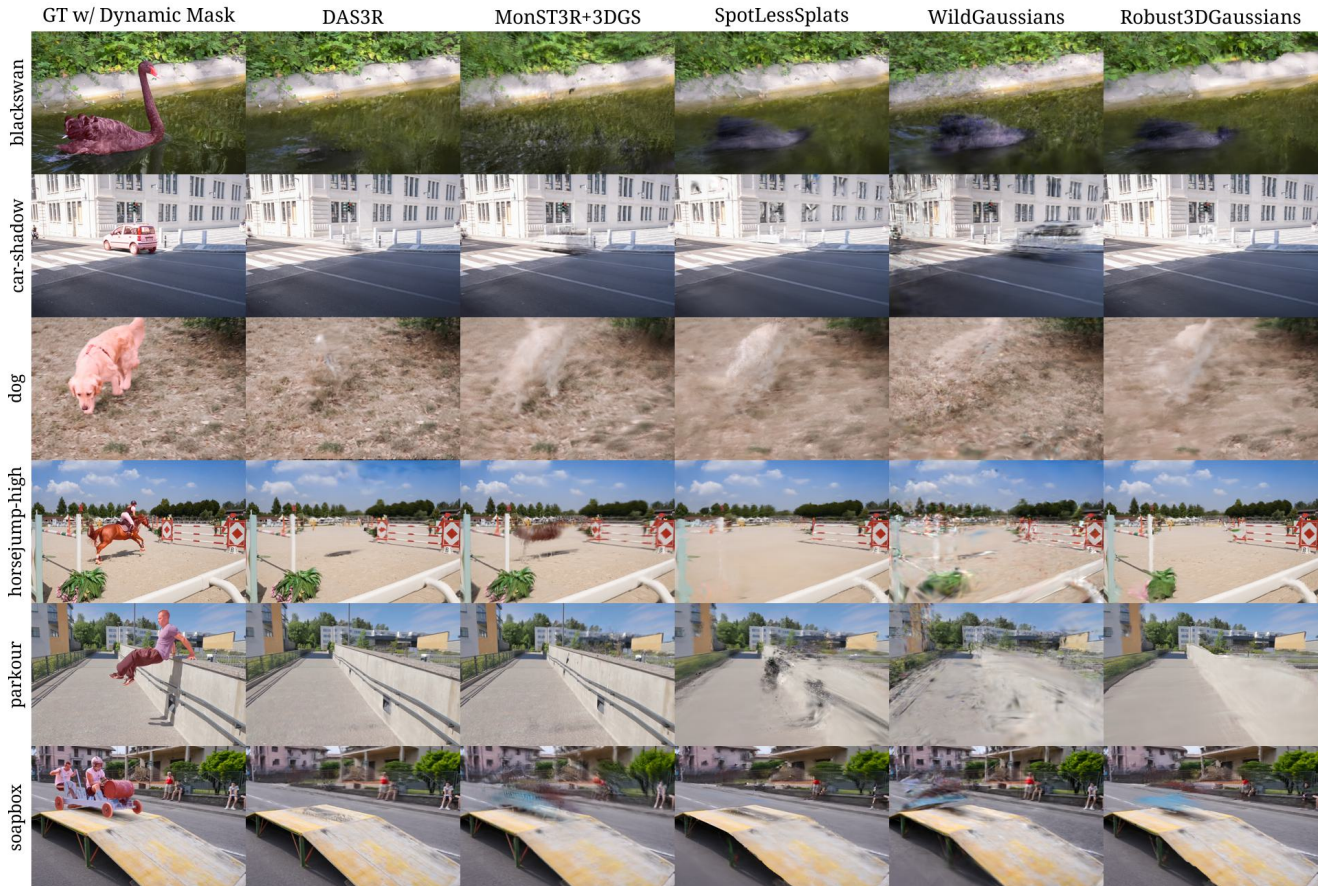
5.3. Static Scene Reconstruction

Comparison on DAVIS and Sintel Dataset We compared the distractor-free Gaussian reconstruction methods employed in unconstrained image sets, including WildGaussians [8], Robust3DGS [24], and SpotLessSplats [18], as well as a pose-free baseline method combining MonST3R [32] and InstantSplat [4]. The camera parameters calculated by COLMAP [19, 20] were used to evaluate the results of the first three methods.

We provide quantitative comparisons for DAVIS dataset in Table 3 and Sintel dataset in Table 4. DAS3R obtains highest average scores even without any camera poses as input. We also provide qualitative comparisons for DAVIS dataset in Figure 4 and Sintel dataset in Figure 5. WildGaussians fails to reconstruct when camera movement is large and a dynamic object takes large camera space, *e.g.* ambush-5 (2nd row of Sintel) and ambush-6 (3rd row of Sintel). Robust3DGS and SpotLessSplats fail to remove dynamic objects once they take a lot of camera space. For some cases, *e.g.* horsejump-high (4th row of DAVIS), SpotLessSplats removes a lot of static content (the hurdles). Our DAS3R is able to correctly detect dynamic objects (even with their shadow and reflection) and remove them accordingly.

Gaussian Splatting training efficiency We also compare the cost of training in Table 5. DAS3R only requires 4000 iterations, while the other methods require at least 30000 iterations, which take 10 minutes to train on a video of length 50.

Figure 4. Qualitative comparison on DAVIS dataset. DAS3R achieves best rendering quality and is able to correctly detect and remove dynamic objects with their shadow and reflection. SpotLessSplats removes static content (the hurdles) in horsejump-high (4th row of DAVIS).



	blackswan	camel	car-shadow	dog	horsejump-high	motocross-jump	parkour	soapbox	Average
WildGaussians	18.95	19.19	21.45	19.74	18.79	7.91	18.89	20.55	18.18
Robust3DGS	19.58	21.31	29.31	22.48	20.87	13.83	21.29	22.55	21.40
SLS-mlp	21.14	25.62	22.77	23.82	18.78	17.82	23.15	22.43	21.94
MonST3R + InstantSplat	20.30	20.97	25.55	24.41	24.38	18.95	25.26	25.35	23.14
DAS3R w/o static conf	24.12	27.06	31.04	28.53	21.11	17.92	26.90	26.11	25.35
DAS3R	23.90	27.27	29.13	28.63	25.09	17.09	28.09	26.41	25.70

Table 3. Comparison on DAVIS dataset. The PSNR is computed on static area by masking out dynamic content. The best results are **bold**. DAS3R achieves best average results, even without COLMAP poses given.

5.4. Dynamic Mask Accuracy

Table 1 presents the accuracy results for the dynamic masks on DAVIS and Sintel, evaluated using IoU accuracy. Figure 2 and Figure 3 show some examples comparing DAS3R and MonST3R’s dynamic mask. Our methods provide more valid masks than MonST3R when there are large dynamic objects. One of the limitations is our method tends to predict false positives on static areas; this could be mitigated by Staticness optimization during Gaussian Splatting training.

5.5. Camera Pose Accuracy

We provide camera pose estimation accuracy from the global alignment step in Table 2. Our method achieves remarkable improvement in Relative Rotation accuracy on Sintel, and all metrics on TUM-dynamics. This result demonstrates the necessity of utilizing more accurate dynamic masks for global camera pose alignment. Better camera poses also provide initialization for training Gaussian Splats.

Figure 5. Qualitative comparison on Sintel dataset. DAS3R is robust to large dynamic objects while other methods fail to remove the dynamic objects and even fail to reconstruct the overall scene .



	alley-2	ambush-4	ambush-5	ambush-6	cave-2	cave-4	market-2	market-5	market-6	shaman-3	sleeping-1	sleeping-2	temple-2	temple-3	Average
WildGaussians	16.75	21.43	7.87	4.02	26.69	27.68	23.14	11.47	16.56	32.29	15.38	17.06	16.50	15.15	18.00
Robust3DGS	17.96	19.18	12.20	10.46	27.70	29.68	22.28	16.85	16.23	35.88	15.58	15.93	12.68	20.68	19.52
SLS-mlp	19.09	19.75	14.14	5.50	27.62	29.20	23.74	17.73	17.76	36.84	19.05	21.61	19.12	22.12	20.95
MonST3R+InstantSplat	27.70	22.51	18.04	14.75	27.40	31.94	27.12	23.57	26.86	43.89	31.20	35.73	28.84	21.00	27.18
DAS3R w/o static conf	31.50	24.61	26.23	18.71	28.32	32.06	28.11	26.41	20.05	44.45	14.98	14.70	21.44	23.78	25.38
DAS3R	31.10	24.52	26.28	19.26	28.32	31.86	29.03	26.49	23.58	45.60	26.30	25.67	27.18	23.90	27.79

Table 4. Comparison on Sintel dataset. The PSNR is computed on static area by masking out dynamic content. The best results are **bold**. DAS3R achieves best average results, even without COLMAP poses given.

	Iterations	Time
DAS3R	4000	~2mins
WildGaussians	70000	~40mins
Robust3DGS	30000	~10mins
SLS-mlp	30000	~10mins

Table 5. Comparison on training cost. Test on RXT 4090 on a 480p video of 50 frames.

5.6. Ablation on Staticness

We verify the effectiveness of Staticness in terms of rendering accuracy of trained Gaussian Splats. Results are provided in Table 3 and Table 5. Disabling Staticness leads to degraded results, especially on hard samples where the network falsely predicts the static content as dynamic objects.

6. Conclusion

This work introduces DAS3R, a novel framework for scene decomposition and static background reconstruction from dynamic monocular videos. By leveraging dynamics-aware Gaussian splatting and accurately predicting dynamic masks through a learning-based approach, DAS3R achieves robust and effective reconstruction in challenging scenarios involving significant dynamic objects and complex camera movements. Compared to prior methods, DAS3R demonstrates superior performance, evidenced by substantial gains in PSNR and enhanced camera pose estimation across benchmark datasets like DAVIS and Sintel. Despite its robustness, the system occasionally suffers from false positives in dynamic object detection, particularly in areas with significant depth variation. Addressing these limitations through more diverse training data and improved model refinements will be the focus of future work.

References

- [1] Ijaz Akhter, Yaser Sheikh, Sohaib Khan, and Takeo Kanade. Nonrigid structure from motion in trajectory space. *Advances in neural information processing systems*, 21, 2008. 2
- [2] Bescos, Berta, FÁCil, JM., Civera, Javier, and José Neira. DynaSLAM: Tracking, mapping and inpainting in dynamic environments. *IEEE RA-L*, 2018. 1, 2
- [3] D. J. Butler, J. Wulff, G. B. Stanley, and M. J. Black. A naturalistic open source movie for optical flow evaluation. In *European Conf. on Computer Vision (ECCV)*, pages 611–625. Springer-Verlag, 2012. 2, 3, 6
- [4] Zhiwen Fan, Wenyan Cong, Kairun Wen, Kevin Wang, Jian Zhang, Xinghao Ding, Danfei Xu, Boris Ivanovic, Marco Pavone, Georgios Pavlakos, et al. InstantSplat: Unbounded sparse-view pose-free gaussian splatting in 40 seconds. *arXiv preprint arXiv:2403.20309*, 2(3):4, 2024. 5, 6
- [5] Martin A. Fischler and Robert C. Bolles. Random sample consensus: A paradigm for model fitting with applications to image analysis and automated cartography. *Commun. ACM*, 24(6):381–395, 1981. 1
- [6] Bernhard Kerbl, Georgios Kopanas, Thomas Leimkühler, and George Drettakis. 3d gaussian splatting for real-time radiance field rendering. *ACM Trans. Graph.*, 42(4):139–1, 2023. 3
- [7] Alexander Kirillov, Eric Mintun, Nikhila Ravi, Hanzi Mao, Chloe Rolland, Laura Gustafson, Tete Xiao, Spencer Whitehead, Alexander C. Berg, Wan-Yen Lo, Piotr Dollár, and Ross Girshick. Segment anything. *arXiv:2304.02643*, 2023. 4
- [8] Jonas Kulhanek, Songyou Peng, Zuzana Kukekova, Marc Pollefeys, and Torsten Sattler. Wildgaussians: 3d gaussian splatting in the wild. *arXiv preprint arXiv:2407.08447*, 2024. 1, 2, 3, 6
- [9] Jiahui Lei, Yijia Weng, Adam W. Harley, Leonidas J. Guibas, and Kostas Daniilidis. Mosca: Dynamic gaussian fusion from casual videos via 4d motion scaffolds. *CoRR*, abs/2405.17421, 2024. 1, 2, 3
- [10] Yiming Li, Zehong Wang, Yue Wang, Zhiding Yu, Zan Gojcic, Marco Pavone, Chen Feng, and Jose M. Alvarez. Memorize what matters: Emergent scene decomposition from multitraverse. In *Advances in Neural Information Processing Systems (NeurIPS)*, 2024. 1
- [11] Jingyu Lin, Jiaqi Gu, Lubin Fan, Bojian Wu, Yujing Lou, Renjie Chen, Ligang Liu, and Jieping Ye. Hybrids: Decoupling transients and statics with 2d and 3d gaussian splatting. In *Arxiv*, 2024. 2, 3
- [12] Yu-Lun Liu, Chen Gao, Andreas Meuleman, Hung-Yu Tseng, Ayush Saraf, Changil Kim, Yung-Yu Chuang, Johannes Kopf, and Jia-Bin Huang. Robust dynamic radiance fields. In *IEEE/CVF Conference on Computer Vision and Pattern Recognition, CVPR 2023, Vancouver, BC, Canada, June 17-24, 2023*, pages 13–23. IEEE, 2023. 1, 2, 3
- [13] Hidenobu Matsuki, Riku Murai, Paul HJ Kelly, and Andrew J Davison. Gaussian splatting slam. In *Proceedings of the IEEE/CVF Conference on Computer Vision and Pattern Recognition*, pages 18039–18048, 2024. 3
- [14] Takashi Otonari, Satoshi Ikehata, and Kiyoharu Aizawa. Entity-nerf: Detecting and removing moving entities in urban scenes. *CVPR*, 2024. 1, 3
- [15] Federico Perazzi, Jordi Pont-Tuset, Brian McWilliams, Luc Van Gool, Markus Gross, and Alexander Sorkine-Hornung. A benchmark dataset and evaluation methodology for video object segmentation. In *Proceedings of the IEEE conference on computer vision and pattern recognition*, pages 724–732, 2016. 2, 3, 6
- [16] René Ranftl, Alexey Bochkovskiy, and Vladlen Koltun. Vision transformers for dense prediction. In *Proceedings of the IEEE/CVF international conference on computer vision*, pages 12179–12188, 2021. 4
- [17] Martin Runz, Maud Buffier, and Lourdes Agapito. Maskfusion: Real-time recognition, tracking and reconstruction of multiple moving objects. In *2018 IEEE International Symposium on Mixed and Augmented Reality (ISMAR)*, pages 10–20. IEEE, 2018. 1, 2
- [18] Sara Sabour, Lily Goli, George Kopanas, Mark Matthews, Dmitry Lagun, Leonidas Guibas, Alec Jacobson, David J Fleet, and Andrea Tagliasacchi. Spotlessplats: Ignoring distractors in 3d gaussian splatting. *arXiv preprint arXiv:2406.20055*, 2024. 1, 2, 3, 6
- [19] Johannes Lutz Schönberger and Jan-Michael Frahm. Structure-from-motion revisited. In *Conference on Computer Vision and Pattern Recognition (CVPR)*, 2016. 6
- [20] Johannes Lutz Schönberger, Enliang Zheng, Marc Pollefeys, and Jan-Michael Frahm. Pixelwise view selection for unstructured multi-view stereo. In *European Conference on Computer Vision (ECCV)*, 2016. 6
- [21] Zachary Teed and Jia Deng. Deepv2d: Video to depth with differentiable structure from motion. In *8th International Conference on Learning Representations, ICLR 2020, Addis Ababa, Ethiopia, April 26-30, 2020*. OpenReview.net, 2020. 2
- [22] Haithem Turki, Jason Y Zhang, Francesco Ferroni, and Deva Ramanan. Suds: Scalable urban dynamic scenes. In *Proceedings of the IEEE/CVF Conference on Computer Vision and Pattern Recognition*, pages 12375–12385, 2023. 3
- [23] Benjamin Ummenhofer, Huizhong Zhou, Jonas Uhrig, Nikolaus Mayer, Eddy Ilg, Alexey Dosovitskiy, and Thomas Brox. Demon: Depth and motion network for learning monocular stereo. In *2017 IEEE Conference on Computer Vision and Pattern Recognition, CVPR 2017, Honolulu, HI, USA, July 21-26, 2017*, pages 5622–5631. IEEE Computer Society, 2017. 2
- [24] Paul Ungermann, Armin Ettenhofer, Matthias Nießner, and Barbara Roessle. Robust 3d gaussian splatting for novel view synthesis in presence of distractors. *arXiv preprint arXiv:2408.11697*, 2024. 1, 2, 3, 4, 6
- [25] Jianyuan Wang, Nikita Karaev, Christian Rupprecht, and David Novotný. Vggsfm: Visual geometry grounded deep structure from motion. In *IEEE/CVF Conference on Computer Vision and Pattern Recognition, CVPR 2024, Seattle, WA, USA, June 16-22, 2024*, pages 21686–21697. IEEE, 2024. 2
- [26] Shuzhe Wang, Vincent Leroy, Johann Cabon, Boris Chidlovskii, and Jérôme Revaud. Dust3r: Geometric 3d

- vision made easy. In *IEEE/CVF Conference on Computer Vision and Pattern Recognition, CVPR 2024, Seattle, WA, USA, June 16-22, 2024*, pages 20697–20709. IEEE, 2024. [2](#), [4](#)
- [27] Shizun Wang, Xingyi Yang, QiuHong Shen, Zhenxiang Jiang, and Xinchao Wang. Gflow: Recovering 4d world from monocular video. *CoRR*, abs/2405.18426, 2024. [3](#)
- [28] Yanan Wang, Kun Xu, Yaobin Tian, and Xilun Ding. Drg-slam: a semantic rgb-d slam using geometric features for indoor dynamic scene. In *2022 IEEE/RSJ International Conference on Intelligent Robots and Systems (IROS)*, pages 1352–1359. IEEE, 2022. [1](#)
- [29] Philippe Weinzaepfel, Thomas Lucas, Vincent Leroy, Yohann Cabon, Vaibhav Arora, Romain Brégier, Gabriela Csurka, Leonid Antsfeld, Boris Chidlovskii, and Jérôme Revaud. CroCo v2: Improved Cross-view Completion Pre-training for Stereo Matching and Optical Flow. In *ICCV*, 2023. [4](#)
- [30] Linhui Xiao, Jinge Wang, Xiaosong Qiu, Zheng Rong, and Xudong Zou. Dynamic-slam: Semantic monocular visual localization and mapping based on deep learning in dynamic environment. *Robotics and Autonomous Systems*, 117:1–16, 2019. [1](#), [2](#)
- [31] Jun Zhang, Mina Henein, Robert Mahony, and Viorela Ila. Vdo-slam: A visual dynamic object-aware slam system. *arXiv preprint arXiv:2005.11052*, 2020. [1](#), [2](#)
- [32] Junyi Zhang, Charles Herrmann, Junhwa Hur, Varun Jampani, Trevor Darrell, Forrester Cole, Deqing Sun, and Ming-Hsuan Yang. Monst3r: A simple approach for estimating geometry in the presence of motion. *arXiv preprint arXiv:2410.03825*, 2024. [1](#), [2](#), [3](#), [4](#), [6](#)
- [33] Yang Zheng, Adam W. Harley, Bokui Shen, Gordon Wetstein, and Leonidas J. Guibas. Pointodyssey: A large-scale synthetic dataset for long-term point tracking. In *ICCV*, 2023. [2](#), [4](#), [6](#)